

Efficient generation of 1096 nm and 1572 nm by simultaneous stimulated Raman scattering and optical parametric oscillation in one KTiOPO₄ crystal

H.T. Huang · J.L. He · S.D. Liu · J.F. Yang · B.T. Zhang ·
F.Q. Liu

Received: 1 June 2010 / Revised version: 2 August 2010 / Published online: 29 December 2010
© Springer-Verlag 2010

Abstract The simultaneous stimulated Raman scattering (SRS) and optical parametric oscillation (OPO) for the 1064 nm radiation were realized in one KTP crystal for the first time. At an incident diode laser power of 8.6 W, the maximum average output powers at 1096 nm and 1572 nm were 1.1 W and 0.36 W, respectively. The conversion efficiency to Stokes with respect to the incident diode power was as high as 12.8%. The corresponding minimum pulse widths at 1096 nm and 1572 nm were 2.8 and 1.1 ns, respectively.

1 Introduction

Simultaneous multiple-wavelength emission is of fundamental scientific interest and has applications in various fields, such as medical treatment, holographic interferometry, and laser spectroscopy. The frequency conversions induced by the nonlinear crystals have been validated as efficient approaches for the multiple-wavelength emission. Gao et al. have achieved the simultaneous RGB output from a 532 nm pumped optical parametric oscillation (OPO) and subsequent frequency mixing in a PPSLT crystal [1]. This corresponds to the cascaded $\chi^{(2)}$ second-order nonlinearities. The cascaded $\chi^{(3)}$ third-order nonlinearities have also been utilized to realize the multiple-wavelength output.

Y.T. Chang et al. have demonstrated an intracavity stimulated Raman scattering (SRS) up to the fourth order [2]. The investigation that combines efficient $\chi^{(2)}$ and $\chi^{(3)}$ frequency conversions in the same crystal is a research field of rapidly growing importance [3–8].

Potassium titanyl phosphate (KTiOPO₄; KTP) has high optical damage threshold, high nonlinear coefficients, wide acceptance angles and thermally stable phase-matching properties, which make it useful for the second harmonic generation (SHG), sum-frequency mixing (SFM), and OPO. G.A. Massey et al. first conducted the Raman scattering studies in KTP, indicating it can be used as the SRS converter devices [9]. Subsequent investigations on Raman scattering in KTP as well as its isomorphs provided substantial amount of data [10–12]. The most prominent Raman shifts of KTP are in the regions of 200–400 cm⁻¹ and 600–850 cm⁻¹. They are associated with the TiO₆ octahedral torsional and stretching modes, respectively. So it is attractive to combine the $\chi^{(2)}$ and $\chi^{(3)}$ nonlinearities in one KTP crystal. Y.F. Chen has reported the efficient second-order SRS conversion with simultaneous self-SFM and self-SHG in one KTP crystal [13]. Enhanced Raman scattering and concurrent Raman oscillation have been observed in a nanosecond PPKTP OPO [14]. However, the subsequent SRS would limit the parametric conversion efficiency.

Coexistent Raman and parametric conversion both for the fundamental wave were also obtained in an x-cut KTiAsO₄ (KTA, isomorph of KTP) [15]. In their work, the OPO was based on the coupled resonator setup, and the SRS enjoyed the shared cavity configuration. In comparison with KTA, KTP has the increased infrared absorption at the wavelength range of 3–4 μm that induced by the high-energy PO₄ groups [16]. However, as reported in reference [14], this “negative” absorption in KTP can enhance the subsequent SRS. The OPO idle wave can be coupled with the second

H.T. Huang · J.L. He (✉) · S.D. Liu · J.F. Yang · B.T. Zhang ·

F.Q. Liu

State Key Laboratory of Crystal Materials, Institute of Crystal Materials, Shandong University, Ji’nan 250100, China

e-mail: jlhe@sdu.edu.cn

H.T. Huang

e-mail: hht840211@163.com

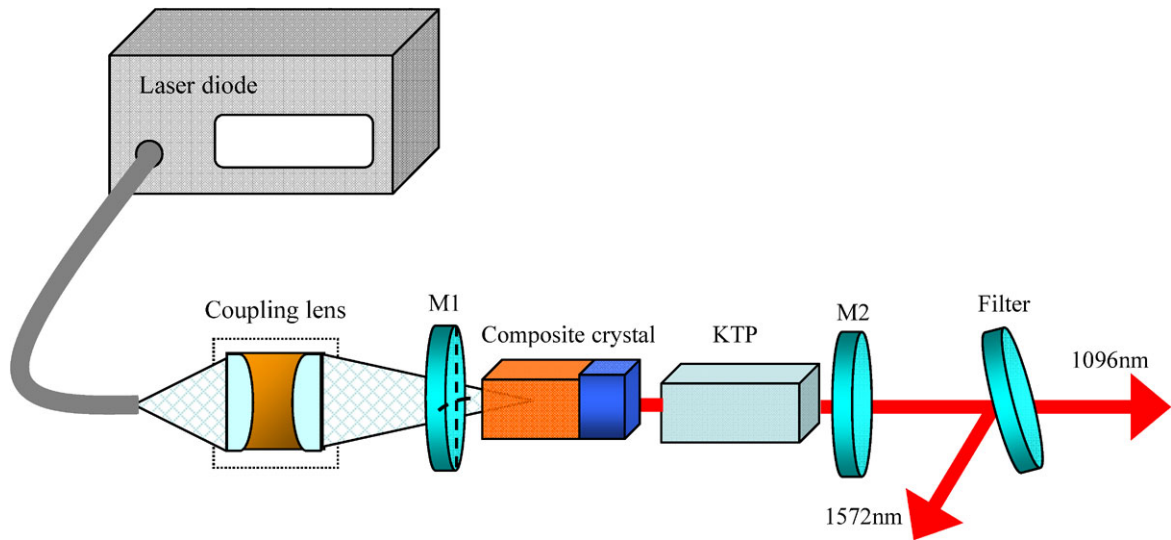


Fig. 1 Schematic diagram of the simultaneous SRS and OPO based on one KTP intracavity pumped by a diode-pumped passively *Q*-switched Nd:YAG/Cr⁴⁺:YAG laser

overtone band for the fundamental vibration of the phosphate ion, resulting in the excitation of vibrational modes of PO₄ groups. Because the structure of KTP consists of chains of interlinked TiO₆ and PO₄ groups, the vibrations in PO₄ can decay into the lower-energy vibrational modes of TiO₆. Therefore, as for the simultaneous SRS and OPO operation, KTP should have an advantage over KTA due to the increased absorption in the wavelength range 3–4 μm.

In this paper, it was demonstrated, for the first time, one KTP crystal simultaneously served as the Raman converter and OPO medium in a compact diode-pumped passively *Q*-switched Nd:YAG/Cr⁴⁺:YAG laser cavity. The OPO signal, Stokes and pump radiation shared the same resonator. At an incident diode laser power of 8.6 W, the maximum average output power at 1096 nm and 1572 nm were 1.1 W and 0.36 W, respectively. The corresponding minimum pulse widths at 1096 and 1572 nm were 2.8 and 1.1 ns, respectively.

2 Experimental setup

The schematic diagram for the compact simultaneous OPO and SRS laser is shown in Fig. 1. The pump source was a fiber-coupled 808 nm diode laser with a core diameter of 0.6 mm and numerical aperture of 0.22. Its radiation was coupled into the laser crystal by a focusing optical system with a 25 mm focal length and 95% coupling efficiency. The radius of the pump beam within the laser crystal was around 300 μm. M1 was a plano-concave mirror with 500 mm radius of curvature. It was antireflection coated at 808 nm ($R < 0.2\%$) on one surface, high-reflection

coated at 1064&1096&1572 nm ($R > 99.8\%$) and high-transmission coated at 808 nm ($T > 90\%$) on the other surface. The output coupler M2 has the high-reflection coating at 1064 nm ($R > 99.8\%$), partial-reflection coating at 1096 nm ($R = 75.7\%$), partial-reflection coating at 1572 nm ($R = 14.1\%$). A plot for the transmission of this output coupler is given in Fig. 2. The composite crystal was comprised of a 1.0 at.% Nd:YAG with the dimensions of 4.5 × 4.5 × 6 mm³ and a 4.5 × 4.5 × 1.5 mm³ Cr⁴⁺:YAG saturable absorber with the initial transmission of 85%. The Cr⁴⁺:YAG was diffusion-bonded to one facet of the Nd:YAG. The x-cut ($\theta = 90^\circ$, $\varphi = 0^\circ$) KTP crystal was with the dimensions of 4 × 4 × 20 mm³, and was antireflection coated at 1572 nm and 1064 nm on both surfaces ($R < 0.2\%$). Both the Nd:YAG/Cr⁴⁺:YAG composite crystal and KTP crystal were wrapped with indium foil and mounted in copper block cooled by water at a temperature of 20°C. The overall cavity length was as short as 30 mm. A filter with high-transmission coating at 1096 nm and high-reflection coating at 1572 nm was used to separate the two wavelengths. The laser pulse was recorded by a Tektronix DPO7104 digital oscilloscope (1 GHz bandwidth, 5 Gs/s sampling rate) and two photodetectors (New focus, model 1611).

3 Experimental results and analysis

Unlike other threshold-less $\chi^{(2)}$ nonlinear frequency conversion processes, such as SHG and SFM, the OPO clearly exhibits a threshold. Moreover, being the $\chi^{(3)}$ frequency conversion, the SRS threshold is generally high. Therefore, a powerful pump source is necessary for the realization of simultaneous SRS and OPO in one KTP. For this purpose, a

Fig. 2 A plot for the transmission of output coupler M2 with the inset displaying the transmissions at 1050–1140 nm

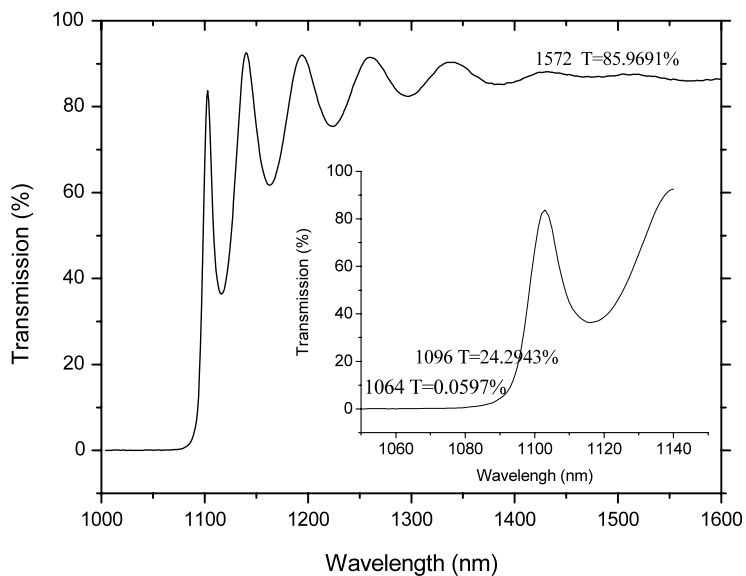
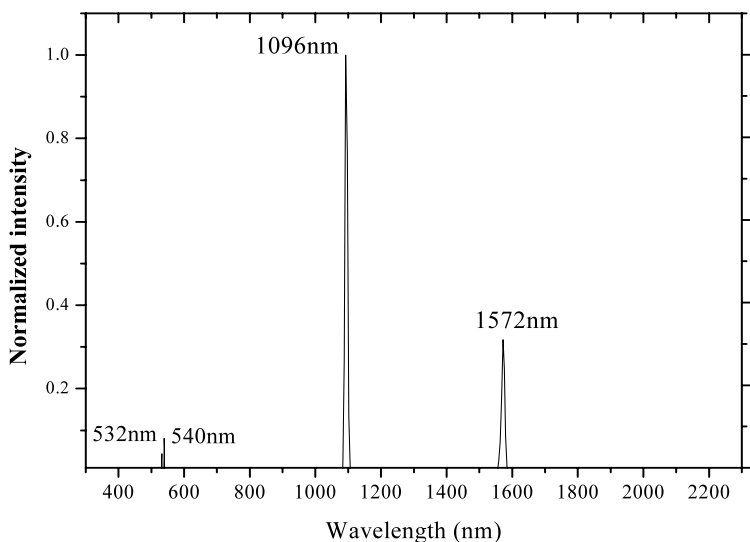


Fig. 3 Optical spectrum of the multiple-wavelength laser



diode-pumped passively *Q*-switched Nd:YAG laser is chosen as the pump source. The $X(Z, Z)X$ Raman configuration can be satisfied in the x-cut KTP. As for the OPO operation, the fundamental radiation with the polarization being parallel to the Y -axis of KTP crystal can be transformed. Consequently, the competition between the SRS and OPO in term of polarizations can be eliminated, which is attributed to the random polarization characteristic of Nd:YAG.

To begin with, an optical spectrum analyzer (AvaSpec-3648-NIR256-2.2) was used to measure the spectral information of the laser output. The present spectrum analyzer was comprised of two synchronized spectrometers, one ranged over 300–1087 nm with the resolution of 0.5 nm and the other ranged over 1087–2100 nm with the resolution of 10 nm. Figure 3 displays the optical spectrum of the laser output in the above two region. The first-order Stokes

induced by the 270 cm^{-1} Raman shift of KTP was located at 1096 nm. As could be seen, the signal wave at 1572 nm resulting from the 1064 nm pumped OPO is also observed in Fig. 3, which validated the realization of simultaneous SRS and OPO in one KTP was practicable. Furthermore, we also observed the weak green output. The peaks were determined to be located at 532 and 540 nm, respectively. This should be attributed to the SHG at 1064 nm and the SFM from the 1064 nm and 1096 nm. Consequently, wide wavelength extension for the fundamental wave was successfully achieved, with the extended wavelengths being at 532, 540, 1096 and 1572 nm. In fact, the KTP simultaneously served as the Raman converter, SHG, SFM and OPO medium in our experiment.

Figure 4 shows the average output powers at 1096 nm and 1572 nm with respect to the incident diode laser power. As

Fig. 4 Average output powers at 1096 and 1572 nm with respect to the incident diode laser power

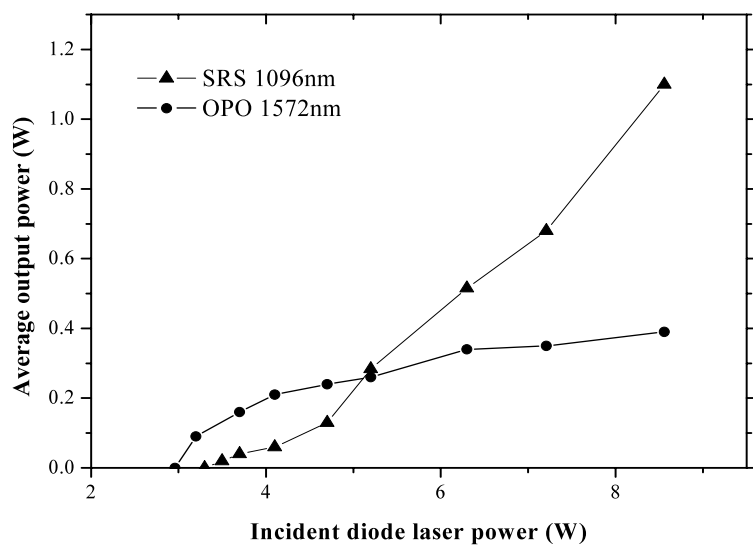
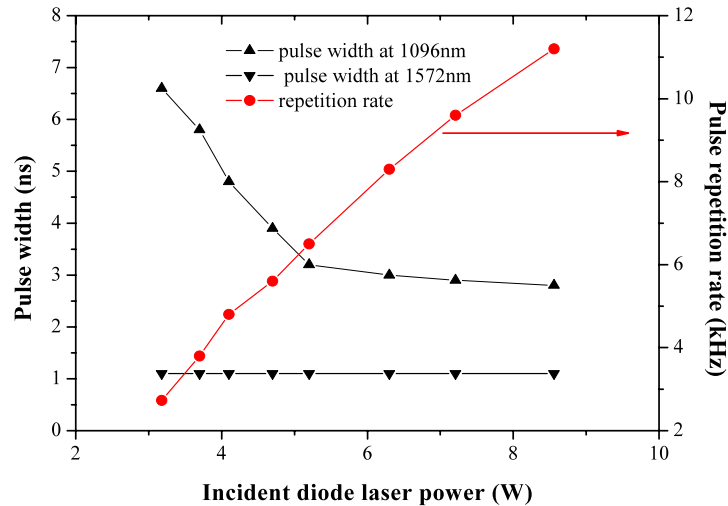


Fig. 5 Pulse widths and repetition rates for 1096 and 1572 nm with respect to the incident diode laser power



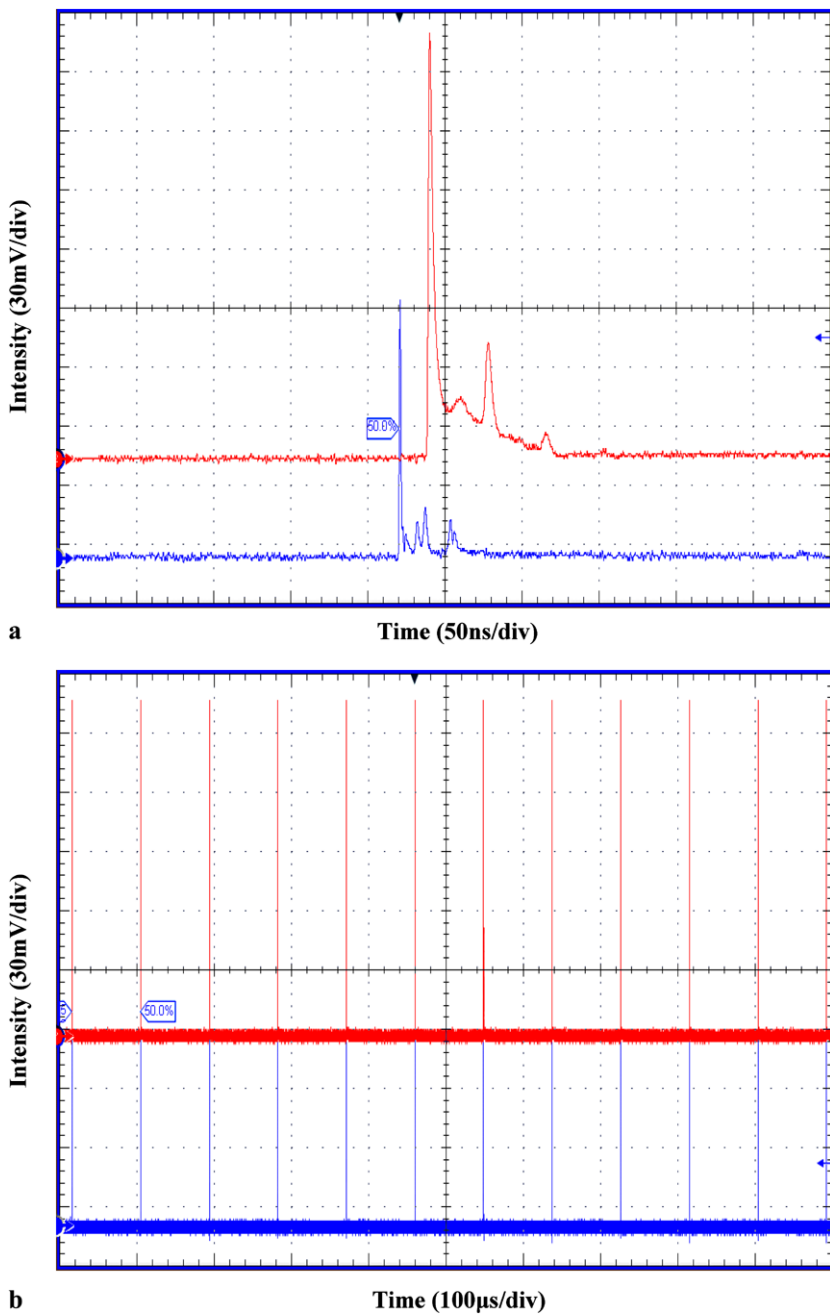
could be seen, the OPO first achieved the threshold at the incident diode laser power of 3.0 W. With the pump power was increased to 3.3 W, the SRS began to oscillate, indicating the realization of simultaneous OPO and SRS. With the help of an additional prism, the observable green output power was estimated to be 15 mW. At an incident diode laser power of 8.6 W, the maximum average output power at 1096 nm and 1572 nm were 1.1 W and 0.36 W, respectively. The total conversion efficiency (Stokes+signal) was estimated to be 17.0% with respect to incident laser diode power. The instability of the average output power at 1096 nm and 1572 nm over hours-long operation was found to be 1.2 and 2.0%, respectively.

Furthermore, considering the fact that the thermally induced birefringence in Nd:YAG could result in the elliptical distribution of the fundamental wave, the KTP was rotated by 90° along X-axis to estimate this influence. Nonetheless, it was found that the first-Stokes power still domi-

nated the total output. We also estimated the performance of the passively *Q*-switched Nd:YAG/Cr⁴⁺:YAG laser with an 1064 nm output coupler. The optimum transmission of the output coupler was found to be approximately 10%. The maximum average output power of 2.1 W was obtained at the incident diode laser power of 9.5 W. The effective first-order Stokes power conversion efficiency with respect to the maximum 1064 nm average output power from the passively *Q*-switched Nd:YAG/Cr⁴⁺:YAG laser was up to 52.4%.

Figure 5 depicts the dependence of pulse widths and repetition rates on the incident diode laser power both for the Stokes and signal. As could be seen, the pulse repetition rates for the two waves are all increased from 3.8 kHz to 11.2 kHz with the diode laser power increased from 3.7 to 8.6 W. It was also found that the pulse width at 1572 nm presented the small variations of 1.3–1.1 ns with increasing the pump power from 3.7 to 8.6 W. This phenomenon was also observed in the single OPO operation, as reported in

Fig. 6 (a) Typical oscilloscope traces for the OPO signal (*the lower*, 1.1 ns pulse width) and Raman pulses (*the upper*, 2.8 ns pulse width). (b) The corresponding pulse trains with 11.2 kHz repetition rates for the OPO signal (*the lower*) and Raman pulses (*the upper*)

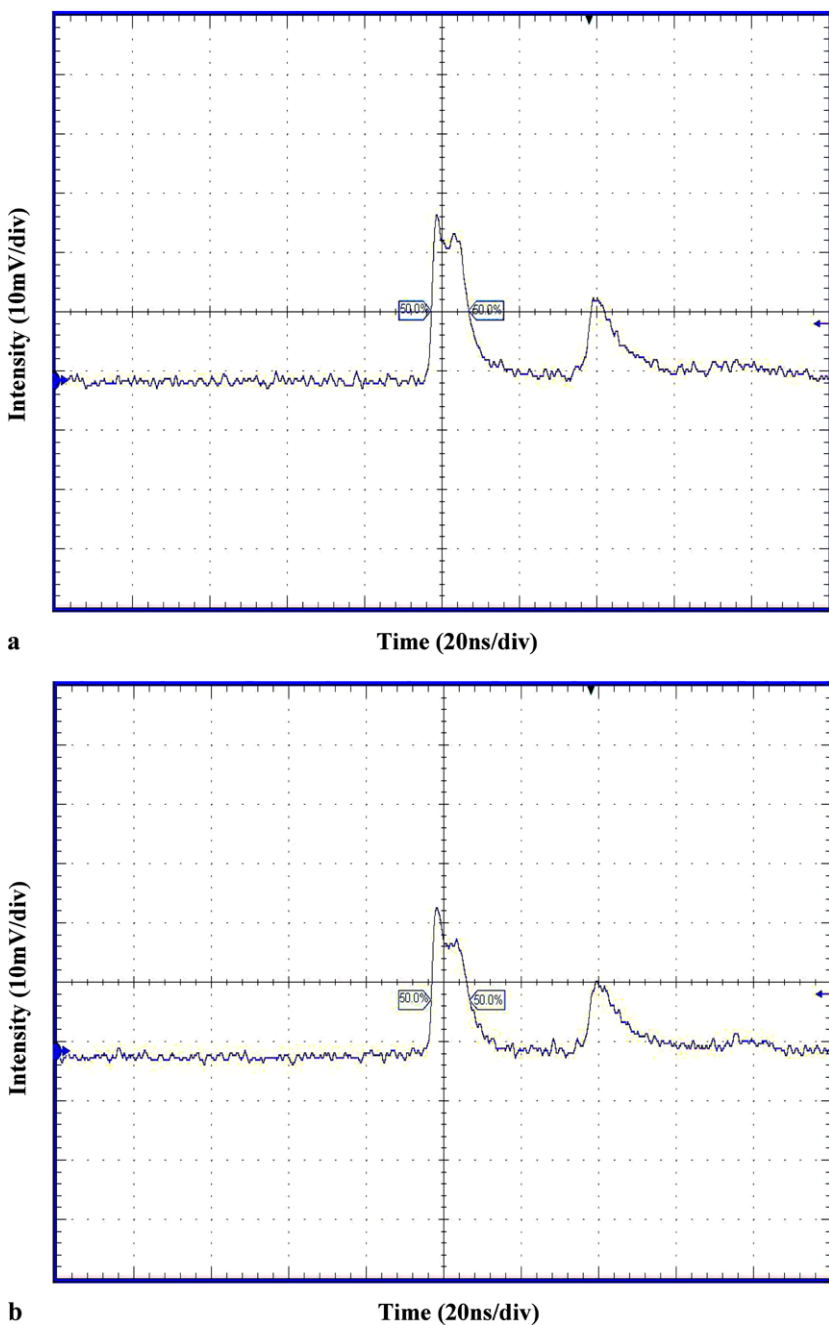


our recent work [17]. The minimum pulse widths at 1096 and 1572 nm were found to be 2.8 and 1.1 ns, respectively. They were greatly shorter than that of 56.3 ns (1535 nm) and 3.5 ns (1091 nm) reported in Ref. [15]. The typical single pulse shape and corresponding pulse trains for the output are shown in Figs. 6a and 6b, respectively. Furthermore, it was also found that the pulse peak-to-peak instability at 1096 nm was superior to that at 1572 nm, with the value being 0.6% and 1.0%, respectively.

The corresponding fundamental pulse traces above the OPO threshold and above the SRS threshold are given in

Fig. 7. Since the parametric gain ($\chi^{(2)}$ nonlinearities) was large, the signal pulse was built up rapidly before the generation of first-order Stokes pulse, resulting in the rapid depletion of the fundamental wave, as shown in Fig. 7a. The following SRS could further deplete the fundamental wave. As can be seen from Fig. 7b, a “platform” occurred in falling edge of the fundamental pulse. The delay between Stokes and parametric signals was 20 ns, as shown in Fig. 6a.

Fig. 7 The corresponding fundamental pulse traces, (a) obtained above the OPO threshold; (b) obtained above the SRS threshold



4 Conclusions

In summary, a novel nonlinear frequency conversion that combined $\chi^{(2)}$ and $\chi^{(3)}$ in one KTP was realized. At an incident diode laser power of 8.6 W, the maximum average output power at 1096 nm and 1572 nm were respectively 1.1 W and 0.36 W, with the conversion efficiency to Stokes with respect to the incident diode power being as high as 12.8%. The corresponding minimum pulse widths at 1096 and 1572 nm were found to be 2.8 and 1.1 ns respectively. The high conversion efficiency, high

peak power and compact size of this simultaneous SRS and OPO laser make it an attractive source for practical applications.

Acknowledgements This work was supported by the National Natural Science Foundation of China (Grant No: 60878012, and 50721002), the Natural Science Foundation of Shandong Province Grant No: 2007ZRB01324, and Program for Taishan Scholars. He Jing-Liang's e-mail address is jlhe@sdu.edu.cn.

References

1. Z.D. Gao, S.N. Zhu, S.-Y. Tu, A.H. Kung, *Appl. Phys. Lett.* **89**, 181101 (2006)
2. Y.T. Chang, Y.P. Huang, K.W. Su, Y.F. Chen, *Opt. Express* **16**, 8286 (2008)
3. A.A. Kaminskii, P. Becker, L. Bohaty, K. Ueda, K. Takichi, J. Hanuza, M. Moczka, H.J. Eichler, G.M.A. Gad, *Opt. Commun.* **206**, 179 (2002)
4. P. Becker, L. Bohatý, R. Fröhlich, H.J. Eichler, K. Ueda, K. Takaichi, J. Hanuza, M. Maczka, H. Rhee, A.A. Kaminskii, *Phys. Status Solidi (a)* **202**, 2543 (2005)
5. A.V. Okishev, J.D. Zuegel, *Opt. Express* **14**, 12169 (2006)
6. A. Henderson, R. Stafford, *Opt. Lett.* **32**, 1281 (2007)
7. Z. Liu, Q. Wang, X. Zhang, S. Zhang, J. Chang, S. Fan, W. Sun, G. Jin, X. Tao, Y. Sun, S. Zhang, Z. Liu, *Opt. Lett.* **34**, 2183 (2009)
8. A.A. Kaminskii, Bohatý, P. Becker, J. Liebertz, L. Bayarjargal, J. Anuza, H.J. Eichler, H. Rhee, J. Dong, *Laser Phys. Lett.* **4**, 660 (2007)
9. G.A. Massey, T.M. Loehr, L.J. Willis, J.C. Johnson, *Appl. Opt.* **19**, 4136 (1980)
10. I. Savatinova, S. Tonchev, T. Popov, E. Liarokapis, C.C. Ziling, *J. Phys. D* **27**, 1384 (1994)
11. D.D. Tuschel, G.R. Paz-Pujalt, W.P. Risk, *Appl. Phys. Lett.* **66**, 1035 (1995)
12. V. Pasiskevicius, C. Canalias, F. Laurell, *Appl. Phys. Lett.* **88**, 041110 (2006)
13. Y.F. Chen, *Opt. Lett.* **30**, 400 (2005)
14. V. Pasiskevicius, A. Fragemann, F. Laurell, R. Butkus, V. Smilgevicius, A. Piskarskas, *Appl. Phys. Lett.* **82**, 325 (2003)
15. Z. Liu, Q. Wang, X. Zhang, Z. Liu, J. Chang, H. Wang, S. Zhang, S. Fan, G. Jin, X. Tao, S. Zhang, H. Zhang, *Opt. Express* **16**, 17092 (2008)
16. J.C. Jacco, G.M. Loiacono, *Appl. Phys. Lett.* **58**, 560 (1991)
17. H.-T. Huang, J.-L. He, J.-F. Yang, B.-T. Zhang, J.-L. Xu, S.-D. Liu, *Appl. Phys. B*. doi:[10.1007/s00340-010-3934-9](https://doi.org/10.1007/s00340-010-3934-9)